AGP polysaccharide chains are required for normal biogenesis of plasmodesmata

Ryoya Okawa, Yoko Hayashi, Yasuko Yamashita, Yoshikatsu Matsubayashi and Mari Ogawa-Ohnishi*

Division of Biological Science, Graduate School of Science, Nagoya University Chikusa, Nagoya 464-8602, Japan
Institute for Glyco-core Research (iGCORE), Nagoya University, Chikusa, Nagoya 464-8601, Japan
*Correspondence to: M. Ogawa-Ohnishi (ohnishi@bio.nagoya-u.ac.jp)

Summary
Arabinogalactan proteins (AGPs) are a plant-specific family of extracellular proteoglycans characterized by large and complex galactose-rich polysaccharide chains. Functional elucidation of AGPs, however, has been hindered by the high degree of redundancy of AGP genes. To uncover as yet unexplored roles of AGPs in *Arabidopsis*, a mutant of Hyp *O*-galactosyltransferase (HPGT), a critical enzyme that catalyzes the common initial step of Hyp-linked arabinogalactan chain biosynthesis, was used. Here we show, using the *hpgt1,2,3* triple mutant, that a reduction in functional AGPs leads to a stomatal patterning defect in which two or more stomata are clustered together. This defect is attributed to increased and dysregulated symplastic transport following changes in plasmodesmata structure, such that highly permeable complex branched plasmodesmata with cavities in branching parts increased in the mutant. We also found that the *hpgt1,2,3* mutation causes a reduction of cellulose in the cell wall and accumulation of pectin, which controls cell wall porosity. Our results highlight the importance of AGPs in the correct biogenesis of plasmodesmata, possibly acting through the regulation of cell wall properties surrounding the plasmodesmata.

Keywords
arabinogalactan protein, Hyp *O*-galactosyltransferase, plasmodesmata, cell wall, *Arabidopsis*.

Significance Statement

There is a growing awareness that arabinogalactan proteins (AGPs) regulate various aspect of plant development, but the highly redundant nature of this family's members often makes it difficult to elucidate their functions by a conventional reverse genetics approach. To sidestep gene redundancy problems, we focused on a mutant of Hyp *O*-galactosyltransferase which catalyzes the initial step in the elongation of complex arabinogalactan chains, and identified previously unknown roles of AGPs in *Arabidopsis*.

Introduction

Arabinogalactan proteins (AGPs) are plant-specific extracellular proteoglycans found widely throughout the plant kingdom, from the green alga *Chlamydomonas* to higher plants (Ma *et al.*, 2017). AGPs are characterized by a high proportion of carbohydrate moieties, which represents more than 90% of the total molecular mass and are thought to be critical for molecular function (Ellis *et al.*, 2010). To date, a total of 151, 282, and 313 putative AGPs have been identified in the model plants *Arabidopsis thaliana*, *Oryza sativa*, and *Glycine max*, respectively. In *Arabidopsis*, 151 AGPs are further classified into five classes based on the similarities in their core protein structures: 23 classical AGPs; 16 arabinogalactan (AG) peptides; three Lys-rich AGPs; four hybrid AGPs; and 105 chimeric AGPs (Ma *et al.*, 2017). AGPs are ubiquitous in all plant organs and thought to perform various functions in each organ (Showalter, 2001, Ellis *et al.*, 2010, Su and Higashiyama, 2018, Leszczuk *et al.*, 2020, Hromadova *et al.*, 2021). To date, however, fewer than 30 AGPs in *Arabidopsis* have been functionally characterized, including SOS5/FLA4 (Shi *et al.*, 2003, Griffiths *et al.*, 2014, Seifert *et al.*, 2014, Basu *et al.*, 2016, Seifert, 2021), FLA11, FLA12 (MacMillan *et al.*, 2010, Ma *et al.*, 2022) and AGP18 (Acosta-Garcia and Vielle-Calzada, 2004, Demesa-Arevalo and Vielle-Calzada, 2013). The available results suggest that AGPs play a range of physiological roles in processes such as reproduction, cell proliferation, pattern formation, growth, and plant-microbe interactions (Gaspar *et al.*, 2004, Nguema-Ona *et al.*, 2007, Nguema-Ona *et al.*, 2013, Pereira *et al.*, 2016, Su and Higashiyama, 2018). However, the high level of genetic and functional redundancy of AGP genes has hindered the elucidation of their specific roles.

Yariv phenylglycosides are often used as cytochemical reagents to perturb the molecular functions of AGPs (Yariv *et al.*, 1962). Yariv reagents selectively and non-covalently bind to the β-1,3-galactan moiety of AGPs, acting as specific functional inhibitors (Kitazawa *et al.*, 2013). Yariv treatment caused the arrest of pollen tube growth (Mollet, 2002), root hair elongation (Marzec *et al.*, 2015), and root growth, accompanied by microtubule disorganization (Nguema-Ona *et al.*, 2007). However, because Yariv reagents are unable to penetrate the plasma membrane, their targets are limited to tissue surface AGPs.

Carbohydrate-degrading enzymes of AGPs are also useful tools for functional analyses of the sugar moieties of AGPs. Transgenic *Arabidopsis* plants expressing a fungal exo-β-1,3-galactanase that specifically hydrolyzes the β-1,3-galactan backbone of type II AGs showed severe tissue disorganization in the hypocotyl and cotyledons, accompanied by a decrease in Yariv reagent reactive AGPs (Yoshimi *et al.*, 2020). This

suggests that the degradation of type II AGs affects the regulation of cell shape; however, it remains unclear whether this is due to the loss of functional AGPs or the result of cryptic activities of the degraded oligosaccharides. Alternative strategies to deal with gene redundancy at the whole-plant level are required for the comprehensive functional analysis of AGPs.

The biosynthesis of AGP involves *O*-galactosylation of hydroxyproline (Hyp) residues, followed by stepwise elongation of the complex sugar chains (Knoch *et al.*, 2014). Given the functional importance of the carbohydrate moiety of AGPs, the biosynthetic enzymes of polysaccharides are attractive targets in comprehensive loss-of-function analyses of AGPs. The majority of polysaccharides are composed of β-1,3 linked D-galactopyranosyl (Gal*p*) chains with β-1,6 linked D-Gal*p* side chains (Tan *et al.*, 2010). The side chains often terminate in L-Ara*f* and other less-abundant sugars, such as L-Fuc*p*, L-Rha*p* and D-Glc*p*A (Haque *et al.*, 2005, Tryfona *et al.*, 2010, Tryfona *et al.*, 2012). There have been several reported cases in which loss of glycosyltransferases that mediate elongation of AG chains has led to tissue-specific phenotypes (Geshi *et al.*, 2013, Knoch *et al.*, 2013, Dilokpimol *et al.*, 2014).

The Hyp *O*-galactosyltransferases (HPGT1 to 3 and GALT2 to 6) are another important class of AGP biosynthesis enzymes, and these enzymes mediate the initial galactosylation of Hyp residues of AGP core proteins (Basu *et al.*, 2013, Basu *et al.*, 2015, Ogawa-Ohnishi and Matsubayashi, 2015, Showalter and Basu, 2016). Disruption of all three *HPGT* genes resulted in a significant decrease in Hyp *O*-galactosylation activity both *in vitro* and *in vivo,* and caused pleiotropic phenotypes such as longer lateral roots, longer root hairs, radial expansion of the cells in the root tip, smaller leaves, shorter inflorescence stems, reduced fertility and shorter siliques (Ogawa-Ohnishi and Matsubayashi, 2015). Multiple *galt2,3,4,5,6* mutants display weaker phenotypes compared with the *hpgt1,2,3* mutant (Zhang *et al.*, 2021); however, the introduction of *galt* mutations into the *hpgt1,2,3* mutant enhanced the phenotype, indicating that the eight members of the CAZy GT31 family have, at least in part, redundant roles in the biosynthesis of AG chains (Kaur *et al.*, 2021). Hyp *O*-galactosylation is a critical step in the elongation of complex AG chains; thus, phenotypes of its loss-of-function mutant should reflect the deficiency in the biosynthesis of all functional AGPs. As yet undiscovered functions of AGPs would be revealed through phenotypic analysis of mutants of enzymes for Hyp *O*-galactosylation.

Here we show, using an *hpgt1,2,3* triple mutant, that a reduction in functional AGPs leads to a stomatal patterning defect in which two or more stomata are clustered together. Our results highlight the importance of AGPs in the correct biogenesis of

plasmodesmata, possibly acting through regulation of the properties of the cell wall surrounding plasmodesmata.

Results

Loss of AGP glycosylation increases stomatal clustering

In order to uncover as yet unexplored roles of AGP, we performed a detailed phenotypic analysis of an *hpgt1,2,3* triple mutant deficient in Hyp *O*-galactosylation, a common initial step for AGP glycosylation. We found that the *hpgt1,2,3* triple mutant displayed stomatal patterning defects; two-six stomata were frequently clustered together in the cotyledon epidermis (Fig. 1a). The percentage of clustered stomata in the *hpgt1,2,3* cotyledon epidermis was 13.3%, which was significantly greater than that in the wild-type control (3.4%). The cluster size was also significantly increased in the *hpgt1,2,3* triple mutant. In the complementation lines in which *HPGT1*, *HPGT2* or *HPGT3* was expressed in the *hpgt1,2,3* triple mutant under the control of the respective promoters, the clustering rate recovered to a degree comparable to that of the wild-type (Fig. 1b, c). These results indicate that AGP glycosylation is critical to the correct spacing and patterning of stomata in the epidermis.

AGP sugar chains affect cell-cell permeability via plasmodesmata

Increased stomatal clustering has also been reported in mutants of KOBITO, a cellulose biosynthetic enzyme, and CHORUS, a callose biosynthetic enzyme, both of which are involved in cell wall polysaccharide biosynthesis (Guseman *et al.*, 2010, Kong *et al.*, 2012). In both cases, plasmodesmata-mediated cell-to-cell movement of cytoplasmic macromolecules was promoted. We therefore hypothesized that the *hpgt1,2,3* triple mutant might also have induced increased intercellular transport via the plasmodesmata. To test this hypothesis, we performed cell-to-cell macromolecular transport assays using cotyledons of the wild-type and *hpgt1,2,3* triple mutant by simultaneously introducing free soluble sGFP (S65T) and endoplasmic reticulum (ER)-targeted monomeric red fluorescent protein (mRFP)-HDEL via particle bombardment. As the HDEL sequence retains mRFP in the ER, mRFP-HDEL serves as an immobile marker of transformed cells. After 16 h of particle bombardment, we observed that 57.4% of the transgenic cells showed diffusion of GFP into the adjacent cells in the *hpgt1,2,3* triple mutant, which was 2.8-fold higher than that in the wild-type (20.9%) (Fig. 2a). A cluster of GFP-positive cells in the *hpgt1,2,3* triple mutant contained up to 14 cells, whereas GFP diffused into 7 cells at most in the wild-type (Fig. 2b). These results suggest that increased stomatal clustering in the *hpgt1,2,3* mutant is due to an increase in plasmodesmata permeability, and raises the possibility that AG chains are necessary for correct formation of plasmodesmata.

AGP sugar chains are essential for correct plasmodesmata formation

To investigate what structural alterations in the plasmodesmata of *hpgt1,2,3* triple mutants cause increased cell-to-cell permeability, we first compared the plasmodesmata density in cotyledon epidermal cells between the wild-type and *hpgt1,2,3* triple mutant. Callose accumulates near the neck of plasmodesmata, and controls their opening and closing (Wu *et al.*, 2018). We stained the callose of cotyledons of the wild-type and *hpgt1,2,3* triple mutant with aniline blue and measured the density of plasmodesmata along the outer periphery of the epidermal cells (Fig. 3a). Fluorescent spot counting revealed the presence of plasmodesmata in the wild-type at 35.4 sites/mm and in the *hpgt1,2,3* triple mutant at 37.2 sites/mm, indicating that there was no difference in plasmodesmata density between the wild-type and mutant (Fig. 3b). We also examined the density of plasmodesmata in cotyledons by expressing the plasmodesmata marker plasmodesmata-located protein 1 (PDLP1)-GFP, which enables visualization of plasmodesmata at higher sensitivity, and we confirmed again that plasmodesmata density was comparable between the wild-type and mutant (Fig. 3c, d).

Next, we observed the morphology of plasmodesmata using transmission electron microscopy (TEM) and classified them into four pattern categories according to shape: simple (simple shape without branching); H-shaped (H-shaped with branching); complex branched (complex shape with many branches without cavities); and large cavity (complex shape with large cavities in branching parts; Fig. 4a-d). Both primary and secondary plasmodesmata are initially simple in structure, and intrinsically form branches or fuse with neighboring plasmodesmata to produce complex structures during tissue development (Ehlers and Kollmann, 2001, Roberts and Oparka, 2003, Faulkner *et al.*, 2008). Notably, we found that the ratio of 'large cavity', the most complex structure, was dramatically increased in the *hpgt1,2,3* triple mutant (27.8%) compared with the wild-type (3.1%; Fig. 4d). These results indicate that loss of AG chains promotes maturation of simple to complex plasmodesmata. Although the relationship between the structure of the plasmodesmata and the cell-to-cell transport efficiency of cytoplasmic macromolecules is not straightforward, the increased intercellular permeability in the *hpgt1,2,3* mutant is highly likely due to structural alterations in the plasmodesmata.

Loss of AGP sugar chains causes an increased proportion of pectin in the cell wall

The pectin-rich cell wall, which is more flexible than cellulose fibers, allows for dynamic changes to the plasmodesmal structure in response to a range of environmental cues. Indeed, plasmodesmata are connected to each other in the middle lamella, a region

particularly rich in pectin and important in adhesion to adjacent cells (Roberts and Oparka, 2003). In our TEM analysis, the middle lamella layer, which is usually observed as a relatively electron-dense region, tended to be less distinguishable in the *hpgt1,2,3* triple mutant than in the wild-type (Fig. 4b,c). This led us to hypothesize that the cell wall composition may be changed in the *hpgt1,2,3* triple mutant.

To examine the composition of the cell wall, cell wall fractions were prepared as alcohol-insoluble residue (AIR) from the cotyledons of the wild-type and *hpgt1,2,3* triple mutant. There was no difference in AIR content between the wild-type and *hpgt1,2,3* triple mutant (Fig. 5a). The fractionation of cell wall polysaccharides by sequential extraction from AIR revealed that the pectin-enriched fraction in the *hpgt1,2,3* triple mutant was increased by 36.8% compared with the wild-type (Fig. 5b). The hemicellulose (HC)-enriched fraction, a supporting material that stabilizes the cell wall, was also slightly increased in the *hpgt1,2,3* triple mutant. In contrast, the cellulose-enriched fraction in the *hpgt1,2,3* triple mutant decreased by 24.3% compared with the wild-type. Analysis of the monosaccharide composition of AIR confirmed that levels of galacturonic acid, galactose, arabinose, xylose and rhamnose, which are major constituents of pectin, were increased in the *hpgt1,2,3* triple mutant (Fig. 5c). Additionally, the total content of calcium ions, which interact with anionic polysaccharide pectin, was 1.6-fold higher in the mutant compared with the wild-type (Fig. 5d). In contrast, levels of glucose, which is the main product of cellulose hydrolysis, were reduced by more than 20% in the *hpgt1,2,3* triple mutant compared with the wild-type (Fig. 5c). These results indicate that loss of AG chains causes a decrease in cellulose proportion and an increase in the pectin proportion in the cell wall.

Discussion

In the present study, we performed a phenotypic analysis of the cotyledons of *hpgt1,2,3*, a mutant defective in Hyp-linked AG chain biosynthesis, and we found that the AGPs are critical for the correct spacing and patterning of stomata in the epidermis. The loss of three HPGTs significantly increased stomatal clustering, a phenotype that has not been described previously in AGP-related mutants. Stomatal development is initiated by the basic helix-loop-helix transcription factor SPEECHLESS (SPCH), which serves as an acceptor of hormonal and environmental signals to regulate stomatal density and patterning during development (MacAlister *et al.*, 2007, Han and Torii, 2016). SPCH does not normally travel in a cell-to-cell manner, but enhanced movement of SPCH to neighboring cells due to increased symplastic connectivity induces stomatal clustering (Guseman *et al.*, 2010, Kong *et al.*, 2012). Because the *hpgt1,2,3* mutant shows increased plasmodesmata permeability of GFP and because the molecular size of SPCH is comparable to that of GFP, it is possible that stomata developed in clusters in the *hpgt1,2,3* mutant as a result of enhanced movement of SPCH to neighboring cells following increased symplastic connectivity.

As plant cells are connected by plasmodesmata, which facilitate the symplastic transport of macromolecules, we expected that the *hpgt1,2,3* triple mutant would exhibit increased intercellular transfer via plasmodesmata. Indeed, we found that the ratio of the 'large cavity' class, the most complex plasmodesmata with large central cavities, was dramatically increased in the *hpgt1,2,3* triple mutant compared with that in the wild-type. Although the relationship between plasmodesmata branching and conductivity is not simple and is often affected by the cell wall environment, symplastic connectivity is reportedly related to changes in the geometry of the plasmodesmata cavity (Oparka *et al.*, 1999, Knox and Benitez-Alfonso, 2014). Increased symplastic transport in *Arabidopsis ise1* and *ise2* mutants is associated with increased X- and Y-shaped and twinned plasmodesmata (Kobayashi *et al.*, 2007, Stonebloom *et al.*, 2009, Burch-Smith and Zambryski, 2010). Computational flow simulations also showed that plasmodesmata with expanded central cavities can be more conductive than plasmodesmata with cylindrical cavities, especially when the cell wall thickness increases (Deinum *et al.*, 2019). Conversely, symplastic transport is restricted in *dse1* mutants, in which the proportion of X- and Y-shaped and twinned plasmodesmata is reduced. These lines of evidence support the theory that more plasmodesmata orifices result in increased symplastic transport (Xu *et al.*, 2012).

Plasmodesmata are often found in a region called the pit field, which is characterized by high pectin and low cellulose content (Faulkner *et al.*, 2008). Pectin has

lower mechanical strength than cellulose (Marga *et al.*, 2003, Phyo *et al.*, 2017), and it is thought to promote the development of secondary plasmodesmata. Analysis of the cell wall composition of the *hpgt1,2,3* triple mutant revealed that the proportion of cellulose was decreased and that of pectin increased. Stomatal patterning defects have also been reported in a mutant of glycosyltransferase-like protein KOBITO1. The *kobito1* mutant shows an increased pectin/cellulose ratio and increased plasmodesmata transport accompanied by increased stomatal clustering (Pagant *et al.*, 2002, Kong *et al.*, 2012, Wang *et al.*, 2015). Therefore, we interpreted these results to indicate that the pectin-rich cell wall environment of the *hpgt1,2,3* triple mutant allows for the facile development of secondary plasmodesmata.

Pectin methylesterase, an enzyme that catalyzes demethylesterification of pectic homogalacturonan, has been shown to localize preferentially around plasmodesmata (Morvan *et al.*, 1998, Knox and Benitez-Alfonso, 2014). Although this demethylesterification can lead to both cell wall strengthening and loosening, depending on the pattern of demethylesterification (Wolf and Greiner, 2012), a high level of demethylesterification generally softens the cell wall and increases cell wall extensibility (Peaucelle *et al.*, 2011, Qi *et al.*, 2017). Pectin is abundant in the middle lamella layer, which is responsible for cell adhesion and appears as a relatively high-electron density area in the cell wall in electron microscopic images. A positive correlation has been reported between the electron density of the middle lamellar region and the extent of calcium-mediated pectin crosslinking (Yan *et al.*, 2022). In the *hpgt1,2,3* triple mutant, the middle lamellar region was often not clearly recognized compared with the wild type in electron microscopy, albeit an increase in pectin proportion in the cell wall was observed. This might suggest that the middle lamella of the *hpgt1,2,3* triple mutant has an increased level of uncrosslinked pectin, which leads to cell wall loosening.

β-Glucosyl-Yariv reagent is known to strongly stain the cell plate, which eventually develops into the middle lamella after cytokinesis, suggesting that AGPs are abundant in the middle lamella as well as in the cell plate (Shibaya and Sugawara, 2009, Yu and Zhao, 2012). AGPs have been proposed as modulators of cell wall mechanics by physically interacting and/or crosslinking with pectin (Seifert and Roberts, 2007). Indeed, AGP57 is covalently linked with pectin via a glycoside linkage (Tan *et al.*, 2013). Loss of AGPs might interfere with correct development of the middle lamella and/or alter its mechano-chemical properties, resulting in the formation of highly permeable plasmodesmata with large central cavities.

Although the function of AG chains in cell wall synthesis and modification remains a topic for debate, several lines of evidence suggest that AGPs positively affect cellulose

biosynthesis. The *cage1cage2* double mutant, a member of the GT31 family putatively involved in the synthesis of the β-1.3-galactans of AGP, showed a 30% decrease in inflorescence cell wall cellulose content compared with the wild type (Nibbering *et al.*, 2022). Plants in which the expression of FLA3, fasciclin-like AGP, was suppressed by RNAi showed abnormal cellulose distribution in the pollen during microspore development (Li *et al.*, 2010). Mutants defective in FLA4/SOS5 function showed a reduction in cellulose biosynthesis in the root tip (Basu *et al.*, 2016). The *Arabidopsis fla11 fla12* double mutant displayed a reduction in cellulose content and tensile strength accompanied by altered cellulose microfibril angle (MacMillan *et al.*, 2010). In contrast, overexpression of FLA12 showed higher cellulose content compared with wild-type plants (Ma *et al.*, 2022). Interestingly, treatment with β-glucosyl-Yariv reagent or antibodies specifically recognizing AGPs caused disorganization of microtubules, which are known to determine the orientation of newly formed cellulose microfibrils, resulting in thicker cortical F-actin filaments, suggesting that microtubule and F-actin organization may depend on the pattern of AGP localization (Sardar *et al.*, 2006, Nguema-Ona *et al.*, 2007).

Comprehensive functional analyses of AGPs have long been hindered by a high degree of redundancy of genes encoding AGPs. We have overcome these limitations by using a loss-of-function mutant for enzymes catalyzing Hyp *O*-galactosylation, a critical step in the elongation of complex AG chains. Phenotypes of this loss-of-function mutant reflect deficiencies in the biosynthesis of the functional AGPs and thus enable us to uncover physiological connections between AGPs and the symplastic permeability of cells. The exact molecular mechanism by which AGP participates in the control of plasmodesmata development remains elusive, but our findings provide the basis for further explorations of AGP functions and cell wall mechano-chemical dynamics.

Experimental procedures

Plant growth conditions

Arabidopsis thaliana ecotype Columbia (Col-0) was used as the wild-type. Loss-of-function homozygous mutants used in this study (*hpgt1-1*, SALK_007547; *hpgt2-1,* SALK_070368; *hpgt3-1*, SALK_009405) were described previously (Ogawa-Ohnishi et al., 2015). For complementation analysis, the full-length *HPGT1*, *HPGT2* and *HPGT3* genomic fragments containing the 2.5-kb promoter region were cloned into the binary vector pIG121-Hm. The primers are listed in Table S1.The constructs were introduced into the *hpgt1,2,3* triple mutant. Surface-sterilized *Arabidopsis* seeds were sown on agar-solidified B5 medium containing 1.0% sucrose, and vernalized for 2 days at 4°C, and then incubated at 22°C under continuous light for the indicated period.

Quantitative analysis of stomatal phenotype

Differential interference contrast microscopy was used to observe the stomatal phenotype on 12-day-old cotyledons of wild-type and *hpgt1,2,3* plants as described. Cotyledons were incubated overnight in a solution of 9:1 ethanol:acetic acid, and then washed in 90, 70, 50, 30 and 0% ethanol for 20 min each. Cotyledons were cleared in a mixture of 8:1:2 chloral hydrate:glycerol:water. For stomatal measurements, the cotyledon epidermis of 15 seedlings was observed, and the epidermal cells, stomata and their cluster size in the center of the cotyledon, excluding the mid-vein region, were quantified using ImageJ software.

Transient transformation of cotyledon epidermis and cell-to-cell mobility assay

Arabidopsis 7-day-old cotyledons were transiently transformed as previously described (Guseman *et al*., 2010). A 1-μg portion of plasmid encoding *proCaMV35S::mRFP-HDEL* and *proCaMV35S::sGFP* was mixed and coated on 0.6-μm gold particles and bombarded using a PDS-1000/He particle delivery system (Bio-Rad) under a rupture-disc pressure of 450 psi. After 12 to 16 h of bombardment, transformed epidermal cells were observed under a confocal laser-scanning microscope (Olympus FV3000) with excitation at 488 nm and 543 nm.

Aniline blue staining

Eight-day-old cotyledons were fixed overnight at 4°C in a solution of 3:1 ethanol:acetic acid. Fixed cotyledons were incubated first for 1 h at 60°C in 1 M sodium phosphate buffer, and then for 2 h at room temperature in 0.01% aniline blue dissolved in 2%

K_3PO_4. The cotyledons were placed in 5% glycerol and observed under an FLUOVIEW FV3000 (Olympus Corp.) confocal laser-scanning microscope with excitation at 405 nm and emission at 440-480 nm.

Expression analysis of PDLP1-GFP

The *PDLP1* ORF and GFP coding regions were ligated in-frame between the *CaMV35S* promoter and *NOS* terminator of the pIG121-Hm vector using an In-Fusion cloning system (Takara Bio Inc., Kusatsu, Japan). Wild-type and *hpgt1,2,3* plants were transformed with *Agrobacterium tumefaciens* strain C58C1 harboring the pIG-*35S:PDLP1-GFP:NOS* vector. The cotyledons were observed under an FLUOVIEW FV3000 (Olympus Corp.) confocal laser-scanning microscope with excitation at 488 nm.

Transmission electron microscopy

Seven-day-old cotyledon fragments (< 2 mm^2) were fixed overnight at 4°C with 2% paraformaldehyde and 2% glutaraldehyde in 0.05 M cacodylate buffer (pH 7.4). Following fixation, the samples were washed three times with 0.05 M cacodylate buffer for 30 min each, and then postfixed for 3 h at 4°C with 2% OsO_4 in 0.05 M cacodylate buffer. Next, the samples were dehydrated in a graded ethanol series (50, 70, 90, and 100%) and infiltrated with propylene oxide (PO) two times for 30 min each and then immersed for 1 h in a 7:3 mixture of PO and resin (Quetol-651; Nisshin EM, Japan). The PO was volatilized overnight, and the samples were transferred to fresh 100% resin and polymerized at 60°C for 48 h. Thin sections (80 nm) were stained with 2% uranyl acetate for 15 min and lead stain solution (Sigma) for 3 min and then observed under a transmission electron microscope (JEM-1400Plus; JEOL, Japan) at 100 kV. TEM was performed by Tokai Electron Microscopy Inc. (Nagoya, Japan).

Preparation of AIR

Eight-day-old cotyledons were freeze-dried and ground to a powder using a Multi-Beads Shocker (Yasui Kikai Corp., Osaka, Japan). The powdered tissue was suspended in aqueous 70% (v/v) ethanol and vortexed. The suspensions were centrifuged at 1300 *g* for 2 min. The insoluble residue was washed three times with a series of 70% ethanol, water, methanol:chloroform (1:1, [v/v]) and acetone, and then air-dried. The starch in the sample was degraded at 37°C for 24 h with 2 units ml^{-1} of *α*-amylase (Sigma-Aldrich Co. LLC., Tokyo, Japan). The suspension was centrifuged

for 2 min at 1300 *g*. The pellet was washed three times with water and then acetone, and finally dried under vacuum.

Fractionation of plant cell walls

AIR (3.0 mg) was treated with 50 mM ethylenediaminetetraacetic acid (pH 6.8) at 95°C for 15 min. The slurry was centrifuged at 9800 *g* for 5 min, and the supernatants from three consecutive extractions were pooled as the pectin-enriched fraction. The residue was then extracted three times at 25°C for 15 min each with 4% and then with 24% KOH containing 0.02% $NaBH_4$. The 4% KOH extracts and 24% KOH extracts were neutralized with acetic acid to obtain an HC1-enriched fraction and HC-2 enriched fraction, respectively. The insoluble residue was then washed three times each with 0.03 N acetic acid and 99.5% ethanol, and dried under vacuum. The cellulose-enriched fraction was dissolved at 25°C for 1 h in 72% (v/v) sulfuric acid and then diluted with a 29-fold volume of water. The total sugar content in each fraction was determined by the phenol sulfuric acid method (Dubois et al. 1956) and expressed as glucose equivalents.

Analysis of cell wall monosaccharide composition

AIR (2.0 mg) was hydrolyzed at 121°C for 1 h in 400 µl of 2 M trifluoroacetic acid (TFA) containing D-ribose (100 µg ml^{-1}) as an internal standard and then cooled at room temperature. The hydrolysates were dried with a centrifugal evaporator at 50°C. The sample was suspended in 400 µl of methanol, dried again, and dissolved in 400 µl of water. After centrifugation at 18 800 *g* for 5 min, the supernatant was collected as the TFA-soluble fraction. The pellet was resuspended in 50 µl of 72% (v/v) sulfuric acid containing D-ribose (800 µg ml^{-1}) as an internal standard. The suspension was incubated at 25°C for 1 h, diluted with 640 µl of water, and boiled at 100°C for 3 h. The hydrolysate was neutralized with $CaCO_3$, and the supernatant was collected as the TFA-insoluble fraction after centrifugation at 18 800 *g* for 5 min. For analysis of monosaccharides, 5 µl of the hydrolysate was incubated at 80°C for 1 h with 20 µl of ABEE labeling kit reagent (J-Oil Mills Inc., Tokyo, Japan). ABEE-labeled monosaccharides were extracted with 400 µl of water/chloroform (1/1 [v/v]), followed by filtration with a DISMIC-13 CP (Advantec Co., Ltd., Tokyo, Japan). Labeled monosaccharides were analyzed by reverse-phase chromatography using a semi-micro HPLC system (PU-2085; Jasco Inc., Tokyo, Japan) equipped with an XBridge C18 column (3.5 µm, 150 mm × 2.1 mm I.D; Waters Corp., Milford, MA, USA) and a fluorescence detector (Ex: 305 nm; Em: 360 nm). Elution was performed with 0.2 M borate-potassium buffer (pH 8.9)/acetonitrile (93/7 [v/v]) at a flow rate of 0.15 ml min^{-1}.

The column temperature was maintained at 50°C. The retention times of the peaks were compared with those of ABEE-monosaccharide standards.

Determination of calcium concentrations in AIR

Calcium concentrations in AIR were measured by inductively coupled plasma mass spectrometry (Agilent 7700x; Agilent Technologies Inc., Santa Clara, CA, USA). These analyses were performed by Japan Testing Laboratories (Ogaki, Japan).

Acknowledgments

This work was supported by JSPS KAKENHI Grant Numbers JP21K20653 to M.O-O. and JP18H05274 and JP20H05907 to Y.M. The authors thank Y. Mizuta and S. Nagahara of Nagoya University for technical advice regarding particle bombardment, and T. Kuroha of the National Agriculture and Food Research Organization for helpful comments.

Supporting Information

Table S1. Primer sequences used in this study.

Conflict of Interest Statement

The authors declare that they have no conflicting interests.

References

Acosta-Garciéa, G. and Vielle-Calzada, J.P. (2004) A classical arabinogalactan protein is essential for the initiation of female gametogenesis in *Arabidopsis*. *Plant Cell*, **16**, 2614-2628. https://doi.org/10.1105/tpc.104.024588

Basu, D., Liang, Y., Liu, X., Himmeldirk, K., Faik, A., Kieliszewski, M., Held, M. and Showalter, A.M. (2013) Functional identification of a hydroxyproline-*O*-galactosyltransferase specific for arabinogalactan protein biosynthesis in *Arabidopsis*. *J Biol Chem*, **288**, 10132-10143. https://doi.org/10.1074/jbc.M112.432609

Basu, D., Tian, L., Debrosse, T., Poirier, E., Emch, K., Herock, H., Travers, A. and Showalter, A.M. (2016) Glycosylation of a Fasciclin-like arabinogalactan-protein (SOS5) mediates root growth and seed mucilage adherence via a cell wall receptor-like kinase (FEI1/FEI2) Pathway in *Arabidopsis*. *PLoS One*, **11**, e0145092. https://doi.org/10.1371/journal.pone.0145092

Basu, D., Wang, W., Ma, S., DeBrosse, T., Poirier, E., Emch, K., Soukup, E., Tian, L. and Showalter, A.M. (2015) Two hydroxyproline galactosyltransferases, GALT5 and GALT2, function in arabinogalactan-protein glycosylation, growth and development in *Arabidopsis*. *PLoS One*, **10**, e0125624. https://doi.org/10.1371/journal.pone.0125624

Burch-Smith, T.M. and Zambryski, P.C. (2010) Loss of INCREASED SIZE EXCLUSION LIMIT (ISE)1 or ISE2 increases the formation of secondary plasmodesmata. *Curr Biol*, **20**, 989-993. https://doi.org/10.1016/j.cub.2010.03.064

Deinum, E.E., Mulder, B.M. and Benitez-Alfonso, Y. (2019) From plasmodesma geometry to effective symplasmic permeability through biophysical modelling. *Elife*, **8**. https://doi.org/10.7554/eLife.49000

Demesa-Arevalo, E. and Vielle-Calzada, J.P. (2013) The classical arabinogalactan protein AGP18 mediates megaspore selection in *Arabidopsis*. *Plant Cell*, **25**, 1274-1287. https://doi.org/10.1105/tpc.112.106237

Dilokpimol, A., Poulsen, C.P., Vereb, G., Kaneko, S., Schulz, A. and Geshi, N. (2014) Galactosyltransferases from Arabidopsis thaliana in the biosynthesis of type II arabinogalactan: molecular interaction enhances enzyme activity. *BMC Plant Biol*, **14**, 90. https://doi.org/10.1186/1471-2229-14-90

Ehlers, K. and Kollmann, R. (2001) Primary and secondary plasmodesmata: structure, origin, and functioning. *Protoplasma*, **216**, 1-30. https://doi.org/10.1007/BF02680127

Ellis, M., Egelund, J., Schultz, C.J. and Bacic, A. (2010) Arabinogalactan-proteins: key regulators at the cell surface? *Plant Physiol*, **153**, 403-419. https://doi.org/10.1104/pp.110.156000

Faulkner, C., Akman, O.E., Bell, K., Jeffree, C. and Oparka, K. (2008) Peeking into pit fields: a multiple twinning model of secondary plasmodesmata formation in tobacco. *Plant Cell*, **20**, 1504-1518. https://doi.org/10.1105/tpc.107.056903

Gaspar, Y.M., Nam, J., Schultz, C.J., Lee, L.Y., Gilson, P.R., Gelvin, S.B. and Bacic, A. (2004) Characterization of the *Arabidopsis* lysine-rich arabinogalactan-protein *AtAGP17* mutant (*rat1*) that results in a decreased efficiency of agrobacterium transformation. *Plant Physiol*, **135**, 2162-2171. https://doi.org/10.1104/pp.104.045542

Geshi, N., Johansen, J.N., Dilokpimol, A., Rolland, A., Belcram, K., Verger, S., Kotake, T., Tsumuraya, Y., Kaneko, S., Tryfona, T., Dupree, P., Scheller, H.V., Hofte, H. and Mouille, G. (2013) A galactosyltransferase acting on arabinogalactan protein glycans is essential for embryo development in Arabidopsis. *Plant J*, **76**, 128-137. https://doi.org/10.1111/tpj.12281

Griffiths, J.S., Tsai, A.Y., Xue, H., Voiniciuc, C., Šola, K., Seifert, G.J., Mansfield, S.D. and Haughn, G.W. (2014) SALT-OVERLY SENSITIVE5 mediates *Arabidopsis* seed coat mucilage adherence and organization through Pectins. *Plant Physiol*, **165**, 991-1004. https://doi.org/10.1104/pp.114.239400

Guseman, J.M., Lee, J.S., Bogenschutz, N.L., Peterson, K.M., Virata, R.E., Xie, B., Kanaoka, M.M., Hong, Z. and Torii, K.U. (2010) Dysregulation of cell-to-cell connectivity and stomatal patterning by loss-of-function mutation in *Arabidopsis CHORUS* (*GLUCAN SYNTHASE-LIKE* 8). *Development*, **137**, 1731-1741. https://doi.org/10.1242/dev.049197

Han, S.K. and Torii, K.U. (2016) Lineage-specific stem cells, signals and asymmetries during stomatal development. *Development*, **143**, 1259-1270. https://doi.org/10.1242/dev.127712

Haque, A., Kotake, T. and Tsumuraya, Y. (2005) Mode of action of beta-glucuronidase from *Aspergillus niger* on the sugar chains of arabinogalactan-protein. *Biosci Biotechnol Biochem*, **69**, 2170-2177. https://doi.org/10.1271/bbb.69.2170

Hromadová, D., Soukup, A. and Tylová, E. (2021) Arabinogalactan proteins in plant roots - An update on possible functions. *Front Plant Sci*, **12**, 674010. https://doi.org/10.3389/fpls.2021.674010

Kaur, D., Held, M.A., Smith, M.R. and Showalter, A.M. (2021) Functional characterization of hydroxyproline-*O*-galactosyltransferases for *Arabidopsis* arabinogalactan-protein synthesis. *Bmc Plant Biol*, **21**, 590. https://doi.org/10.1186/s12870-021-03362-2

Kitazawa, K., Tryfona, T., Yoshimi, Y., Hayashi, Y., Kawauchi, S., Antonov, L., Tanaka, H., Takahashi, T., Kaneko, S., Dupree, P., Tsumuraya, Y. and Kotake, T. (2013) beta-galactosyl Yariv reagent binds to the beta-1,3-galactan of arabinogalactan proteins. *Plant Physiol*, **161**, 1117-1126. https://doi.org/10.1104/pp.112.211722

Knoch, E., Dilokpimol, A. and Geshi, N. (2014) Arabinogalactan proteins: focus on carbohydrate active enzymes. *Front Plant Sci*, **5**, 198. https://doi.org/10.3389/fpls.2014.00198

Knoch, E., Dilokpimol, A., Tryfona, T., Poulsen, C.P., Xiong, G., Harholt, J., Petersen, B.L., Ulvskov, P., Hadi, M.Z., Kotake, T., Tsumuraya, Y., Pauly, M., Dupree, P. and Geshi, N. (2013) A beta-glucuronosyltransferase from *Arabidopsis thaliana* involved in biosynthesis of type II arabinogalactan has a role in cell elongation during seedling growth. *Plant J*, **76**, 1016-1029. https://doi.org/10.1111/tpj.12353

Knox, J.P. and Benitez-Alfonso, Y. (2014) Roles and regulation of plant cell walls surrounding plasmodesmata. *Curr Opin Plant Biol*, **22**, 93-100. https://doi.org/10.1016/j.pbi.2014.09.009

Kobayashi, K., Otegui, M.S., Krishnakumar, S., Mindrinos, M. and Zambryski, P. (2007) *INCREASED SIZE EXCLUSION LIMIT 2* encodes a putative DEVH box RNA helicase involved in plasmodesmata function during *Arabidopsis* embryogenesis. *Plant Cell*, **19**, 1885-1897. https://doi.org/10.1105/tpc.106.045666

Kong, D., Karve, R., Willet, A., Chen, M.K., Oden, J. and Shpak, E.D. (2012) Regulation of plasmodesmatal permeability and stomatal patterning by the glycosyltransferase-like protein KOBITO1. *Plant Physiol*, **159**, 156-168. https://doi.org/10.1104/pp.112.194563

Leszczuk, A., Kalaitzis, P., Blazakis, K.N. and Zdunek, A. (2020) The role of arabinogalactan proteins (AGPs) in fruit ripening-a review. *Hortic Res*, **7**, 176. https://doi.org/10.1038/s41438-020-00397-8

Li, J., Yu, M., Geng, L.L. and Zhao, J. (2010) The fasciclin-like arabinogalactan protein gene, *FLA3*, is involved in microspore development of *Arabidopsis*. *Plant J*, **64**, 482-497. https://doi.org/10.1111/j.1365-313X.2010.04344.x

Ma, Y., MacMillan, C.P., de Vries, L., Mansfield, S.D., Hao, P., Ratcliffe, J., Bacic, A. and Johnson, K.L. (2022) FLA11 and FLA12 glycoproteins fine-tune stem secondary wall properties in response to mechanical stresses. *New Phytol*, **233**, 1750-1767. https://doi.org/10.1111/nph.17898

Ma, Y., Yan, C., Li, H., Wu, W., Liu, Y., Wang, Y., Chen, Q. and Ma, H. (2017) Bioinformatics prediction and evolution analysis of arabinogalactan proteins in the plant kingdom. *Front Plant Sci*, **8**, 66. https://doi.org/10.3389/fpls.2017.00066

MacAlister, C.A., Ohashi-Ito, K. and Bergmann, D.C. (2007) Transcription factor control of asymmetric cell divisions that establish the stomatal lineage. *Nature*, **445**, 537-540. https://doi.org/10.1038/nature05491

MacMillan, C.P., Mansfield, S.D., Stachurski, Z.H., Evans, R. and Southerton, S.G. (2010) Fasciclin-like arabinogalactan proteins: specialization for stem biomechanics and cell wall architecture in *Arabidopsis* and *Eucalyptus*. *Plant J*, **62**, 689-703. https://doi.org/10.1111/j.1365-313X.2010.04181.x

Marga, F., Gallo, A. and Hasenstein, K.H. (2003) Cell wall components affect mechanical properties: studies with thistle flowers. *Plant Physiol Biochem*, **41**, 792-797. https://doi.org/10.1016/S0981-9428(03)00120-7

Marzec, M., Szarejko, I. and Melzer, M. (2015) Arabinogalactan proteins are involved in root hair development in barley. *J. Exp. Bot.*, **66**, 1245-1257. https://doi.org/10.1093/jxb/eru475

Mollet, J., Kim, S., Jauh, GY. et al. (2002) Arabinogalactan proteins, pollen tube growth, and the reversible effects of Yariv phenylglycoside. *Protoplasma*, **219**, 89-98. https://doi.org/10.1007/s007090200009

Morvan, O., Quentin, M., Jauneau, A., Mareck, A. and Morvan, C. (1998) Immunogold localization of pectin methylesterases in the cortical tissues of flax hypocotyl. *Protoplasma*, **202**, 175-184. https://doi.org/10.1007/BF01282545

Nguema-Ona, E., Bannigan, A., Chevalier, L., Baskin, T.I. and Driouich, A. (2007) Disruption of arabinogalactan proteins disorganizes cortical microtubules in the root of *Arabidopsis thaliana*. *Plant J*, **52**, 240-251. https://doi.org/10.1111/j.1365-313X.2007.03224.x

Nguema-Ona, E., Vicre-Gibouin, M., Cannesan, M.A. and Driouich, A. (2013) Arabinogalactan proteins in root-microbe interactions. *Trends Plant Sci*, **18**, 440-449. https://doi.org/10.1016/j.tplants.2013.03.006

Nibbering, P., Castilleux, R., Wingsle, G. and Niittylä, T. (2022) CAGEs are Golgi-localized GT31 enzymes involved in cellulose biosynthesis in *Arabidopsis*. *Plant J*, **110**, 1271-1285. https://doi.org/10.1111/tpj.15734

Ogawa-Ohnishi, M. and Matsubayashi, Y. (2015) Identification of three potent hydroxyproline *O*-galactosyltransferases in *Arabidopsis*. *Plant J*, **81**, 736-746. https://doi.org/10.1111/tpj.12764

Oparka, K.J., Roberts, A.G., Boevink, P., Santa Cruz, S., Roberts, L., Pradel, K.S., Imlau, A., Kotlizky, G., Sauer, N. and Epel, B. (1999) Simple, but not branched, plasmodesmata allow the nonspecific trafficking of proteins in developing tobacco leaves. *Cell*, **97**, 743-754. https://doi.org/10.1016/S0092-8674(00)80786-2

Pagant, S., Bichet, A., Sugimoto, K., Lerouxel, O., Desprez, T., McCann, M., Lerouge, P., Vernhettes, S. and Höfte, H. (2002) *KOBITO1* encodes a novel plasma membrane protein necessary for normal synthesis of cellulose during cell expansion in *Arabidopsis*. *Plant Cell*, **14**, 2001-2013. https://doi.org/10.1105/tpc.002873

Peaucelle, A., Braybrook, S.A., Le Guillou, L., Bron, E., Kuhlemeier, C. and Höfte, H. (2011) Pectin-induced changes in cell wall mechanics underlie organ initiation in *Arabidopsis*. *Curr Biol*, **21**, 1720-1726. https://doi.org/10.1016/j.cub.2011.08.057

Pereira, A.M., Lopes, A.L. and Coimbra, S. (2016) Arabinogalactan proteins as interactors along the crosstalk between the pollen tube and the female tissues. *Front Plant Sci*, **7**, 1895. https://doi.org/10.3389/fpls.2016.01895

Phyo, P., Wang, T., Kiemle, S.N., O'Neill, H., Pingali, S.V., Hong, M. and Cosgrove, D.J. (2017) Gradients in wall mechanics and polysaccharides along growing inflorescence stems. *Plant Physiol*, **175**, 1593-1607. https://doi.org/10.1104/pp.17.01270

Qi, J., Wu, B., Feng, S., Lü, S., Guan, C., Zhang, X., Qiu, D., Hu, Y., Zhou, Y., Li, C., Long, M. and Jiao, Y. (2017) Mechanical regulation of organ asymmetry in leaves. *Nat Plants*, **3**, 724-733. 10.1038/s41477-017-0008-6

Roberts, A.G. and Oparka, K.J. (2003) Plasmodesmata and the control of symplastic transport. *Plant Cell Environ*, **26**, 103-124. https://doi.org/10.1046/j.1365-3040.2003.00950.x

Sardar, H.S., Yang, J. and Showalter, A.M. (2006) Molecular interactions of arabinogalactan proteins with cortical microtubules and F-actin in Bright Yellow-2 tobacco cultured cells. *Plant Physiol*, **142**, 1469-1479. https://doi.org/10.1104/pp.106.088716

Seifert, G.J. (2021) The FLA4-FEI pathway: A unique and mysterious signaling module related to cell wall structure and stress signaling. *Genes (Basel)*, **12**. https://doi.org/10.3390/genes12020145

Seifert, G.J. and Roberts, K. (2007) The biology of arabinogalactan proteins. *Annu Rev Plant Biol*, **58**, 137-161. https://doi.org/10.1146/annurev.arplant.58.032806.103801

Seifert, G.J., Xue, H. and Acet, T. (2014) The *Arabidopsis thaliana FASCICLIN LIKE ARABINOGALACTAN PROTEIN 4* gene acts synergistically with abscisic acid signalling to control root growth. *Ann Bot*, **114**, 1125-1133. https://doi.org/10.1093/aob/mcu010

Shi, H., Kim, Y., Guo, Y., Stevenson, B. and Zhu, J.K. (2003) The *Arabidopsis SOS5* locus encodes a putative cell surface adhesion protein and is required for normal cell expansion. *Plant Cell*, **15**, 19-32. https://doi.org/10.1105/tpc.007872

Shibaya, T. and Sugawara, Y. (2009) Induction of multinucleation by beta-glucosyl Yariv reagent in regenerated cells from *Marchantia polymorpha* protoplasts and involvement of arabinogalactan proteins in cell plate formation. *Planta*, **230**, 581-588. https://doi.org/10.1007/s00425-009-0954-y

Showalter, A.M. (2001) Arabinogalactan-proteins: structure, expression and function. *Cell Mol Life Sci*, **58**, 1399-1417. https://doi.org/10.1007/PL00000784

Showalter, A.M. and Basu, D. (2016) Glycosylation of arabinogalactan-proteins essential for development in *Arabidopsis*. *Commun Integr Biol*, **9**, e1177687. https://doi.org/10.1080/19420889.2016.1177687

Stonebloom, S., Burch-Smith, T., Kim, I., Meinke, D., Mindrinos, M. and Zambryski, P. (2009) Loss of the plant DEAD-box protein ISE1 leads to defective mitochondria and increased cell-to-cell transport *via* plasmodesmata. *Proc Natl Acad Sci U S A*, **106**, 17229-17234. https://doi.org/10.1073/pnas.09092291

Su, S. and Higashiyama, T. (2018) Arabinogalactan proteins and their sugar chains: functions in plant reproduction, research methods, and biosynthesis. *Plant Reprod*, **31**, 67-75. https://doi.org/10.1007/s00497-018-0329-2

Tan, L., Eberhard, S., Pattathil, S., Warder, C., Glushka, J., Yuan, C., Hao, Z., Zhu, X., Avci, U., Miller, J.S., Baldwin, D., Pham, C., Orlando, R., Darvill,

A., Hahn, M.G., Kieliszewski, M.J. and Mohnen, D. (2013) An *Arabidopsis* cell wall proteoglycan consists of pectin and arabinoxylan covalently linked to an arabinogalactan protein. *Plant Cell*, **25**, 270-287. https://doi.org/10.1105/tpc.112.107334

Tan, L., Varnai, P., Lamport, D.T., Yuan, C., Xu, J., Qiu, F. and Kieliszewski, M.J. (2010) Plant *O*-hydroxyproline arabinogalactans are composed of repeating trigalactosyl subunits with short bifurcated side chains. *J Biol Chem*, **285**, 24575-24583. https://doi.org/10.1074/jbc.M109.100149

Tryfona, T., Liang, H.C., Kotake, T., Kaneko, S., Marsh, J., Ichinose, H., Lovegrove, A., Tsumuraya, Y., Shewry, P.R., Stephens, E. and Dupree, P. (2010) Carbohydrate structural analysis of wheat flour arabinogalactan protein. *Carbohydr Res*, **345**, 2648-2656. https://doi.org/10.1016/j.carres.2010.09.018

Tryfona, T., Liang, H.C., Kotake, T., Tsumuraya, Y., Stephens, E. and Dupree, P. (2012) Structural characterization of *Arabidopsis* leaf arabinogalactan polysaccharides. *Plant Physiol*, **160**, 653-666. https://doi.org/10.1104/pp.112.202309

Wang, X., Jing, Y., Zhang, B., Zhou, Y. and Lin, R. (2015) Glycosyltransferase-like protein ABI8/ELD1/KOB1 promotes *Arabidopsis* hypocotyl elongation through regulating cellulose biosynthesis. *Plant Cell Environ*, **38**, 411-422. https://doi.org/10.1111/pce.12395

Wolf, S. and Greiner, S. (2012) Growth control by cell wall pectins. *Protoplasma*, **249 Suppl 2**, S169-175. https://doi.org/10.1007/s00709-011-0371-5

Wu, S.W., Kumar, R., Iswanto, A.B.B. and Kim, J.Y. (2018) Callose balancing at plasmodesmata. *J Exp Bot*, **69**, 5325-5339. https://doi.org/10.1093/jxb/ery317

Xu, M., Cho, E., Burch-Smith, T.M. and Zambryski, P.C. (2012) Plasmodesmata formation and cell-to-cell transport are reduced in *decreased size exclusion limit 1* during embryogenesis in *Arabidopsis*. *Proc Natl Acad Sci U S A*, **109**, 5098-5103. https://doi.org/10.1073/pnas.1202919109

Yan, R., Han, C., Fu, M., Jiao, W. and Wang, W. (2022) Inhibitory effects of $CaCl_2$ and pectin methylesterase on fruit softening of Raspberry during cold storage. *Horticulturae*, **8**. https://doi.org/10.3390/horticulturae8010001

Yariv, J., Rapport, M.M. and Graf, L. (1962) The interaction of glycosides and saccharides with antibody to the corresponding phenylazo glycosides. *Biochem J*, **85**, 383-388. https://doi.org/10.1042/bj0850383

Yoshimi, Y., Hara, K., Yoshimura, M., Tanaka, N., Higaki, T., Tsumuraya, Y. and Kotake, T. (2020) Expression of a fungal exo-beta-1,3-galactanase in

Arabidopsis reveals a role of type II arabinogalactans in the regulation of cell shape. *J Exp Bot*, **71**, 5414-5424. https://doi.org/10.1093/jxb/eraa236

Yu, M. and Zhao, J. (2012) The cytological changes of tobacco zygote and proembryo cells induced by beta-glucosyl Yariv reagent suggest the involvement of arabinogalactan proteins in cell division and cell plate formation. *Bmc Plant Biol*, **12**, 126. https://doi.org/10.1186/1471-2229-12-126

Zhang, Y., Held, M.A., Kaur, D. and Showalter, A.M. (2021) CRISPR-Cas9 multiplex genome editing of the hydroxyproline-*O*-galactosyltransferase gene family alters arabinogalactan-protein glycosylation and function in *Arabidopsis*. *Bmc Plant Biol*, **21**, 16. https://doi.org/10.1186/s12870-020-02791-9

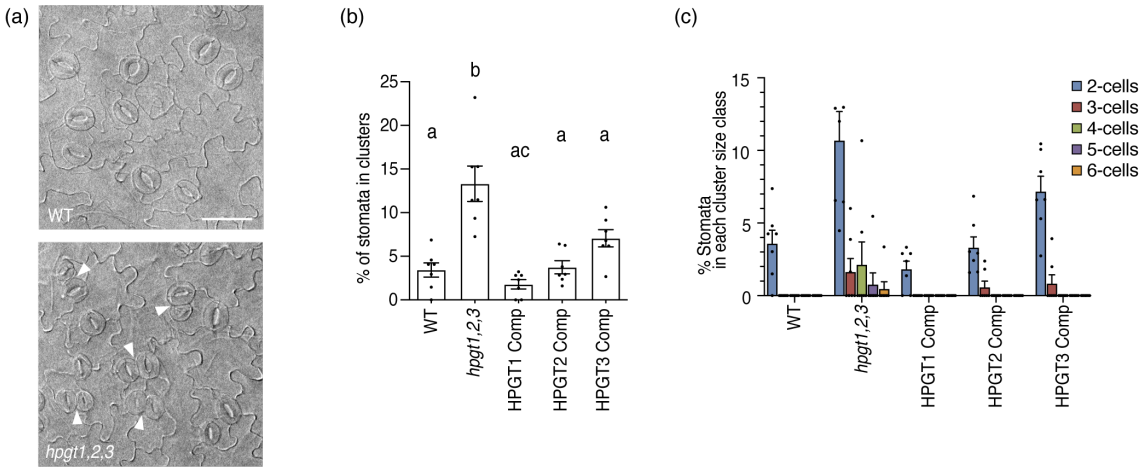

Fig. 1. The *hpgt1,2,3* triple mutant exhibits a stomatal patterning defect. (a) Differential interference contrast images are shown of the abaxial cotyledon epidermis from 12-day-old seedlings. The white arrowheads indicated clustered stomata. Scale bar, 50 µm. (b) Quantification of clustered stomata on the abaxial epidermis of 12-day-old cotyledons in the wild-type, *hpgt1,2,3* triple mutant, and mutant complemented with HPGTs (mean ± SEM, $p < 0.05$, one-way ANOVA followed by Tukey's test, $n = 70$). (c) Percentage of stomata in each cluster size class. Abaxial cotyledons from 12-day-old seedlings of the wild-type, *hpgt1,2,3* triple mutant, and mutant complemented with HPGTs (mean ± SEM, $n = 70$). HPGT, Hyp *O*-galactosyltransferase.

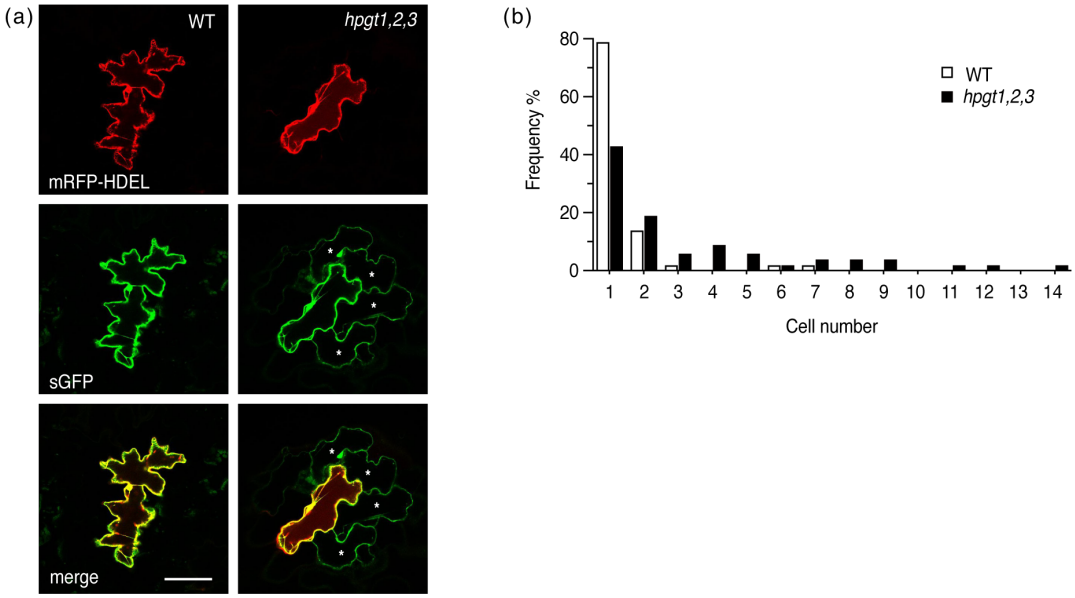

Fig. 2. The *hpgt1,2,3* triple mutant exhibits increased plasmodesmata conductivity. (a) Representative images of the epidermis of cotyledons of 7-day-old seedlings expressing co-bombarded endoplasmic reticulum (ER) localized monomeric red fluorescent protein (mRFP; top), sGFP (S65T; middle), and both merged (bottom). Cells with a less-intense GFP signal are labeled with asterisks. Scale bar: 100 µm. (b) Quantitative distribution analysis of the number of cells expressing GFP per site (n = 50-54).

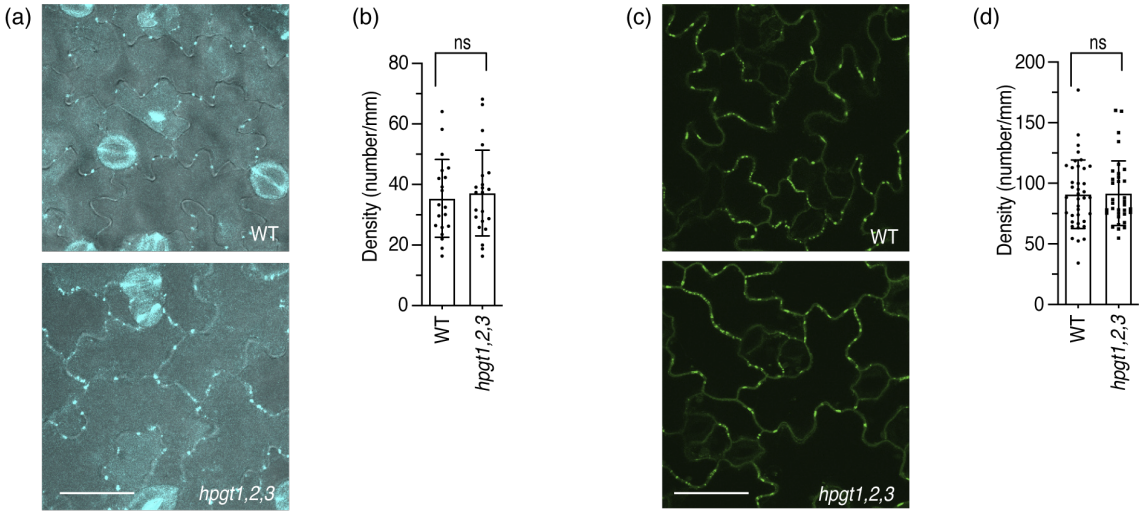

Fig. 3. Plasmodesmata density does not change in the *hpgt1,2,3* triple mutant. (a) Aniline blue staining of plasmodesmal callose in the wild-type and *hpgt1,2,3* triple mutant. Scale bar: 50 µm. (b) Density of callose deposits by aniline blue staining in the wild-type and *hpgt1,2,3* triple mutant (mean ± SD, $p < 0.05$, Student's *t*-test, $n = 20$-22). (c) Confocal micrographs showing the cotyledon epidermis of 8-day-old seedlings expressing plasmodesmata-located protein 1 (PDLP1)-green fluorescent protein (GFP). Scale bar: 50 µm. (d) Density of PDLP1-GFP dots in the wild-type and *hpgt1,2,3* triple mutant (mean ± SD, $p < 0.05$, Student's *t*-test, $n = 34$-38).

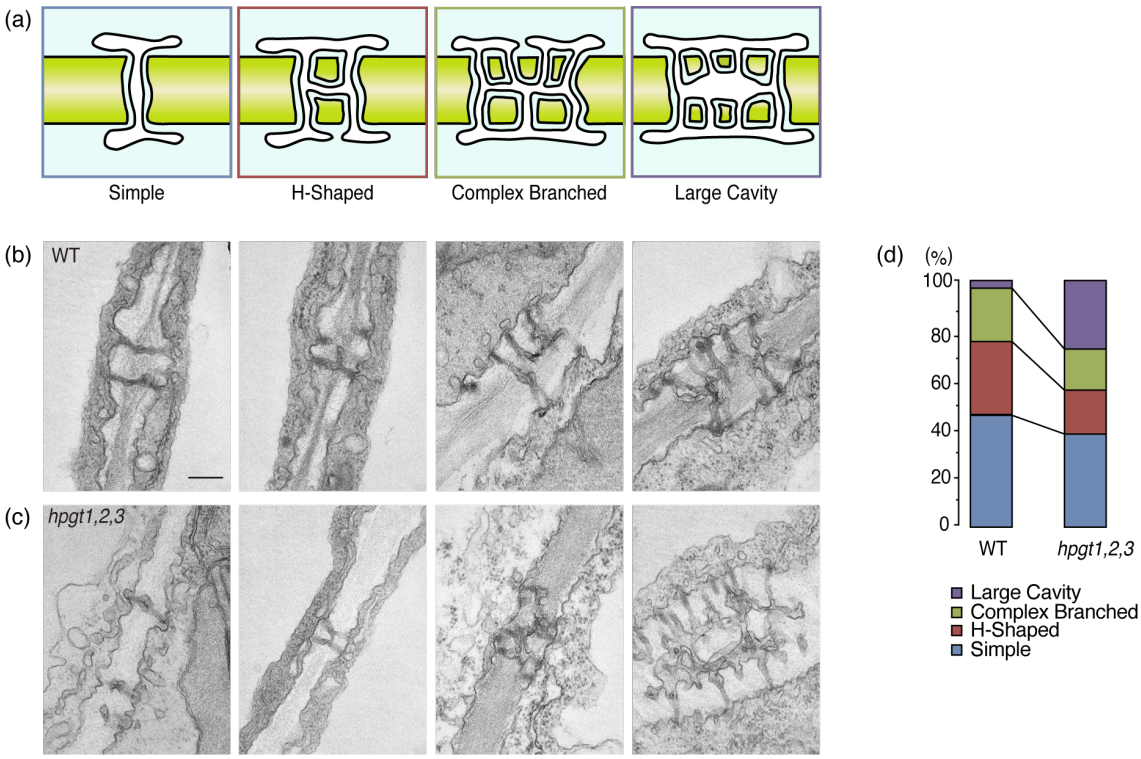

Fig. 4. The *hpgt1,2,3* triple mutant exhibits increased plasmodesmata with highly complex structures. (a) Classification of plasmodesmata structures. (b) Transmission electron microscope (TEM) images. Classification of plasmodesmata in cotyledons of 7-day-old wild-type: simple, H-shaped, complex branched, and large cavity (from left to right). Scale bar: 200 nm. (c) TEM images. Classification of plasmodesmata in cotyledons of 7-day-old *hpgt1,2,3* triple mutants: simple, H-shaped, complex branched, and large cavity (from left to right). (d) Fractions of classified structures of plasmodesmata in the wild-type and *hpgt1,2,3* triple mutant (n = 90-97).

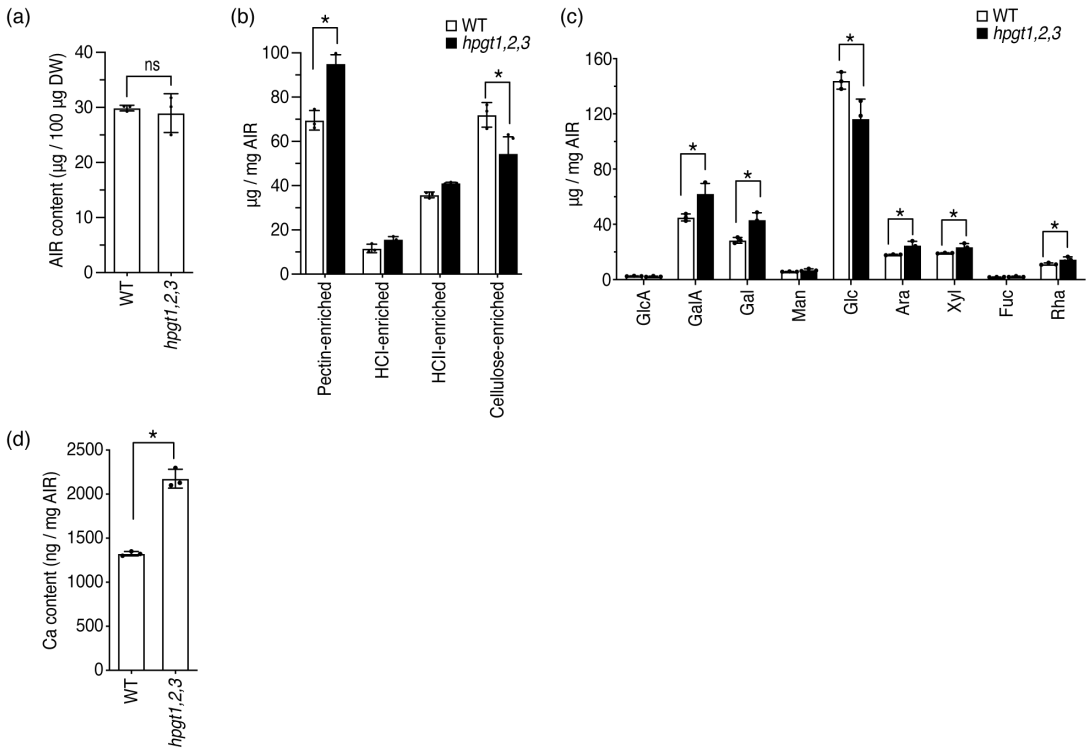

Fig. 5. The *hpgt1,2,3* triple mutant exhibits altered cell wall carbohydrate composition. (a) Comparison of alcohol-insolube residue (AIR) content in 8-day-old cotyledons of the wild-type and *hpgt1,2,3* triple mutant (mean ± SD, $p < 0.05$, Student's *t*-test, $n = 3$). (b) Quantitative comparison of total sugar content in fractions after sequential extraction of AIR from 7-day-old cotyledons of wild-type and *hpgt1,2,3* triple mutants (mean ± SD, $*p < 0.05$, two-way ANOVA followed by Sidak's multiple comparison test, $n = 3$). (c) Quantitative comparison of cell wall monosaccharide composition of 7-day-old cotyledons of the wild-type and *hpgt1,2,3* triple mutant (mean ± SD, $*p < 0.05$, two-way ANOVA followed by Sidak's multiple comparison test, $n = 3$). (d) Quantitative comparison of calcium (Ca) content of 7-day-old cotyledon AIR in the wild-type and *hpgt1,2,3* triple mutant (mean ± SD, $*p < 0.05$, Student's *t*-test, $n = 3$).

Supplementary Table 1. Primer sequences used in this study.					
Experiment	**Forward primer sequence (5'-3')**	**Reverse primer sequence (5'-3')**	**Vector**	**Restriction site**	**Note**
HPGT1 complementation	GCAGGTCGACTCTAGGAACACCTTCTCCTGATACATCTCTGC	GATCGGGGAAATTCGGTAATTAGCTTTCTTCAGAC	pIG121Hm	Xba I, Sac I	In-fusion
HPGT2 complementation	GCAGGTCGACTCTAGCGTTATCTCCAAGTTTTGGGGTTTG	GATCGGGGAAATTCGCATAAACTGTAATGAATGG	pIG121Hm	Xba I, Sac I	In-fusion
HPGT3 complementation	GCAGGTCGACTCTAGGATCGGCCTGCAATAGGCATC	GATCGGGGAAATTCGCGCTATGAATATACGAGTG	pIG121Hm	Xba I, Sac I	In-fusion
proCaMV35S::mRFP-HDEL	CTCTAGAGGATCCCCATGAAGACTAATCTTTTTCT	ATTCGAGCTCGGTACCCTCAAAGCTCATCGTGGTG	pUC-35S:NOS	Sma I	Assembly
proCaMV35S::sGFP	CACGGGGGACTCTAGGATCCCCCGGGCTGCAG	GATCGGGGAAATTCGCGCTTTACTTGTACAGCTCGTC	pUC-35S:NOS	Xba I, Sac I	In-fusion
PDLP1a for pIG-35S:PDLP1a-GFP:NOS	GCAGGTCGACTCTAGTCTTCCAGAGAGCTAATAGC	GAATTCCTGCAGCCCATAAGCATCATATTTATTAC	pIG121Hm	Xba I, Sac I	In-fusion
GFP for pIG-35S:PDLP1a-GFP:NOS	GGGCTGCAGGAATTCGATCCCATG	GATCGGGGAAATTCGCGCTTTACTTGTACAGCTCGTC	pIG121Hm	Xba I, Sac I	In-fusion